Intermittency and coherent structures in a swirling flow: A wavelet analysis of joint pressure and velocity measurements

Pierre Chainais, Patrice Abry, and Jean-François Pinton
Laboratoire de Physique–CNRS URA 1325, Ecole Normale Supérieure de Lyon, 46, allée d'Italie, 69364 Lyon cedex 7, France

(Received 1 December 1998; accepted 15 July 1999)

This work is a contribution to the analysis of intermittency in turbulence, and more precisely of its relation with the existence of coherent structures in the flow. We perform joint in time and space measurements of velocity and pressure in a swirling flow. We detect strong pressure drops on the pressure time series, and study the statistics of the interarrivals of the drops. We then perform a statistical analysis of the pressure and velocity signals, conditioned to the list of detected pressure drops. This allows us to show that the detected drops can be associated with the existence of coherent structures in the flow, whose time patterns, in pressure and velocity, can be deeply connected to these of a filamentary vortex. The wavelet transform allows us to separate the velocity signal into a background phase and a filament phase. We analyze intermittency in terms of log-infinitely divisible cascade models. To do so we rewrite the structure functions, the extended self-similarity ansatz and the log-infinitely divisible cascades formalism in the wavelet framework and discuss the relations between these approaches and intermittency. We show that both the complete velocity signal and its filament or background phases are well described by a log-infinitely divisible cascade. Filaments do influence intermittency: They act on the way the cascade develops along the scales but they do not modify the elementary step of the cascade. © *1999 American Institute of Physics.* [S1070-6631(99)00811-9]

I. INTRODUCTION

It is now a well established fact that coherent structures are observed in turbulent flows, in the sense that, for instance, distinct geometrical properties characterize regions of high dissipation or large vorticity.[1] However, it remains a challenge to relate, in a quantitative manner, the dynamics of these structures to the statistical characteristics of the turbulent cascade. This is a difficult task because it involves inputing information of geometrical nature into a probabilistic description. It is possible in numerical simulations, at least in principle, because the entire flow field is available; however, it is not so straightforward experimentally. Two approaches have been developed: The first one consists in calculating statistical averages of *geometrical quantities* such as the relative direction of representative vectors; the other one is to carry out *conditional averaging*: One identifies a geometrical structure and then computes statistical averages accordingly.

The first approach, performed in numerical[2] and experimental studies[3,4] has shown the importance of alignment effects, such as of vorticity and the eigenvectors of the rate of strain tensor, vorticity and the vortex stretching vector, etc. Emphasis was made on regions of organized vorticity (i.e., structured), rather than on regions of high enstrophy (vorticity modulus). It has also been recently observed that most of the alignment properties are recovered using Burgers' models of a single vortex or a shear layer.[5] That is, alignment effects are linked to the existence of individual objects.

In the second approach, i.e., conditional averaging, the crucial point is the detection of the coherent structures. An option is to build a ''detector,'' using signal processing techniques, from the signal itself that will be conditionally averaged. One searches for events with a particular shape,[6] or with a large amplitude,[7,8] or insulates events of large energy content.[9] The advantage is that detector and signal are directly correlated; it is also the main drawback: The results may be biased *a priori* by the choice of the ''detector.''

In this paper, we use a separate detector, built from an independent measurement. We generate a turbulent swirling flow in a closed vessel and record simultaneously the pressure at a point on the lateral wall and the velocity close to it. The pressure signal is used as a detector for the presence of vorticity filaments; the velocity field is the object of our study. This procedure has the advantage to use a detector which is clearly linked to geometrical objects. Indeed, in this type of flow, the correlation between low pressure events and filamentary vortices has been established in several studies.[10,11] We will show that the velocity field is sensitive to the passage of filaments in its neighborhood and calculate statistical quantities conditioned to the presence of filamentary structures.

Beside the fact that they can be detected by an independent measurement, the choice of conditioning to filaments is motivated by several observations. They have attracted much interest in regards to intermittency since they were first seen in numerical simulations[12] and visualized in experiments:[13] They are regions of enhanced vorticity and dissipation[1,14–16] and they locally violate Kolmogorov's scaling since they accommodate velocity differences of the order of u_{rms} over a scale separation λ (the Taylor micro-scale).[11,17,18] They are

 © 1999 American Institute of Physics

very robust objects which survive the rapid fluctuations of the strain field of a turbulence.[19] Moreover, as already mentioned, the alignment properties observed in turbulent flows can stem from the local influence of coherent vorticity structures. Very intense large scale vortices have recently been shown to have an influence over the turbulent cascade to smaller scales.[5,20] It has been proposed[6,21] that very small filamentary vortices (length λ and core size η, the Kolmogorov scale) control most of the intermittency in the inertial range.

Our analysis uses the wavelet framework rather than the traditional increment description. Wavelets are nowadays widely used for the study of turbulence.[9,22–24] Here, our main motivations are the following. First, wavelet coefficients and increments share the intuition of analysis of the data at a given time scale. More precisely, the increments can actually be exactly rewritten as wavelet coefficients obtained with a wavelet consisting of the difference of δ functions (or Dirac masses), see Sec. IV. Such a wavelet is poor: It is very irregular, it has a quite low spectral localization and it has only one vanishing moment. Wavelet coefficients, therefore, constitute generalizations of increments in various respects. The use of wavelets with more regularity and better joint time/frequency resolution results in a better achievement of the data analysis at a given precise time scale. Using wavelets with a higher number of vanishing moments also results in wavelet coefficients with better statistical properties. There is a quasi-uncorrelation of the wavelet coefficients despite the slow decrease in the autocorrelation function of the data in turbulence. Second, the wavelet transform has been shown to be a relevant tool for the study of scaling properties in time series or systems. It allows to precisely detect the existence of scaling and provides an efficient framework for the estimation of scaling parameters. Thanks to the inherited properties of the wavelet coefficients, theoretical confidence intervals for the estimates can be derived, relying on mild assumptions on the data. Finally, varying the number of vanishing moments of the mother wavelet is a key feature of the wavelet generalization of the increments. It offers a natural way to give robustness to the detection–estimation of scaling since the results should not depend on the *a priori* choice of the mother-wavelet. It also brings robustness in the data analysis against various possibly superimposed noises, corrupting the data. For a review on wavelets and scaling, see Refs. 23, 25, and 26.

We will return to most of these points during the discussion of our results in the following sections. The paper is organized as follows: in Sec. II we describe our experimental setup, measurement techniques and the general flow characteristics; in Sec. III we detail the detection technique, we present a statistical analysis of the waiting times between pressure drops, and we give the average velocity pattern, conditioned to the occurrence of strong pressure drops; in Sec. IV we introduce the wavelet-based structure functions and a log-infinitely divisible cascade model to discuss the influence of vorticity filaments on the intermittency of turbulence.

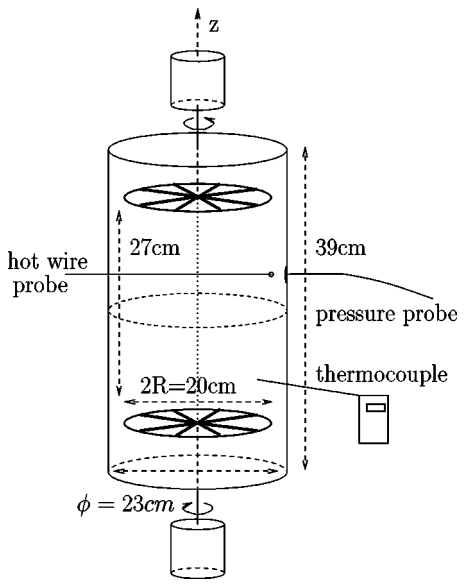

FIG. 1. Experimental set up. The pressure and velocity probes are located 2 cm above the mid-plane of the flow.

II. EXPERIMENTAL SETUP

The experimental setup is sketched in Fig. 1. The flow is produced in the gap between two counter rotating discs, and enclosed in a cylindrical vessel—the von Kármán geometry.[27] This arrangement is known to produce a strong turbulence in a compact region of space.[10,11,28,29]

In our experiment, air is the working fluid; the discs have a diameter $2R=20$ cm and are set 27 cm apart; in order to increase dragging, they are fitted with a set of eight vertical blades, 2 cm high; the enclosing cylinder has a diameter of 23 cm and is 39 cm long. The discs are driven by two independent, 450 Watts, $d.c.$ motors. They rotate in opposite directions at equal rates, adjustable in the range $F_{\mathrm{rot}} \in [10,40]$ Hz. It is kept at a constant value using a tachometry feedback loop with a stability better than 0.1%. Pressure and velocity measurements are made close to the wall, in the vicinity of the mid-plane of the flow. The pressure probe is a 5 mm PCBH112A21 piezoelectric transducer, mounted flush with the lateral wall. It is acceleration compensated; its active diameter is 2.1 mm, its low frequency cutoff at -5% is 0.05 Hz and its rise time is 25 μs. Local velocity measurements are performed using a TSI IFA100 constant temperature anemometer driving a TSI1260A-10 hot-film probe with a sensitive element 10 μm thick and 0.5 mm long; in this situation one essentially measures the modulus of the velocity component perpendicular to the hot-film axis.[30] The hot-film probe constants are determined in a separate calibration wind tunnel; correction are applied to take into account the temperature effects due to the global heating of the fluid inside the vessel. The velocity probe is placed very near the pressure sensor, its position and orientation being finely adjustable. Velocity and pressure records with 1 048 576 data points are stored using a HP 23 bits digitizer; in order to resolve the finer details of the fields, the sampling frequency is set to 78125 Hz.

In the regimes studied here the discs rotate at a nominal

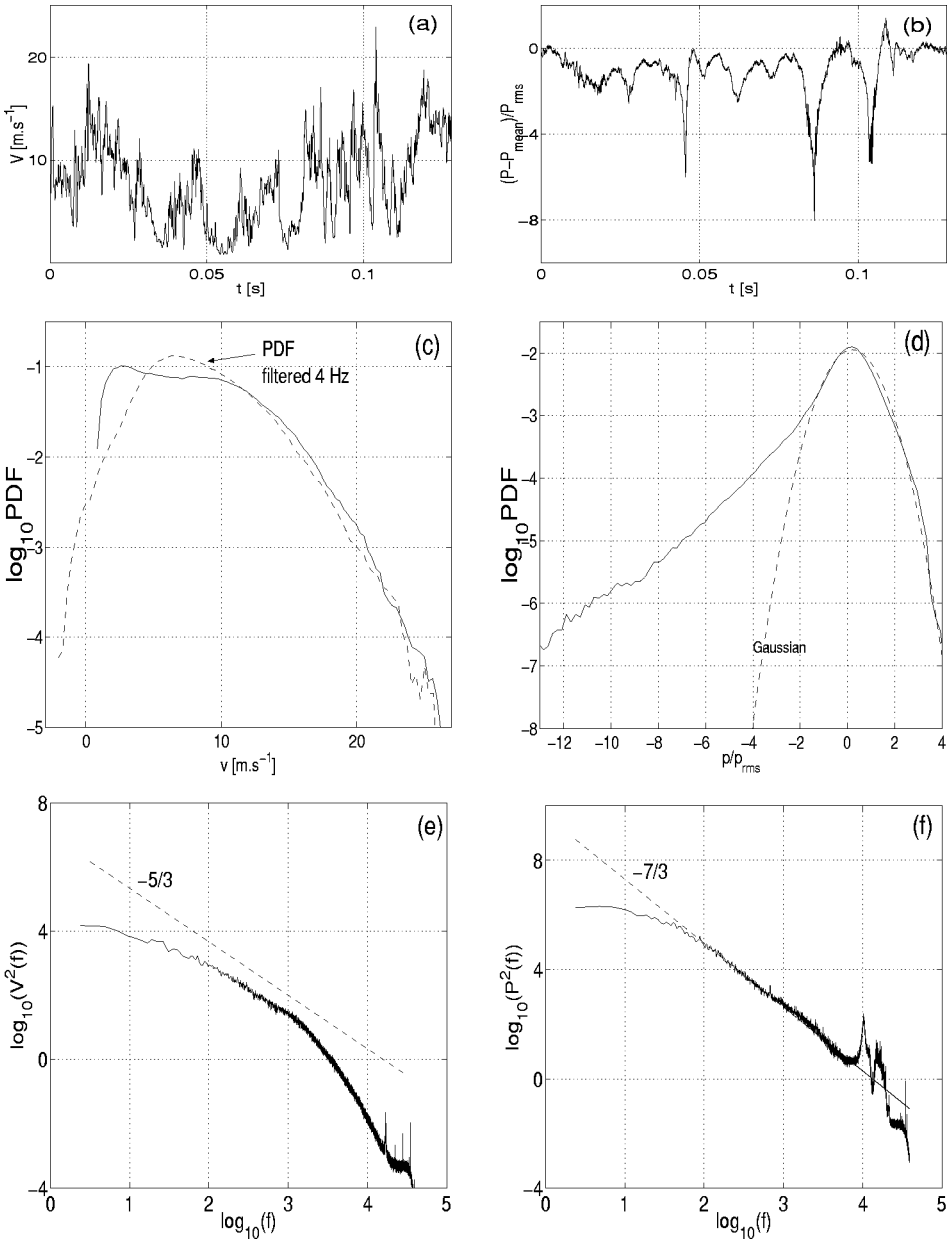

FIG. 2. Flow characteristics. (a) velocity signal; (b) pressure signal; (c) and (d): Corresponding PDFs; (e) and (f) corresponding power spectra. For all recordings, $F_{\mathrm{rot}}=30$ Hz.

frequency of 30 Hz, so that the integral Reynolds number $R_e=R^2\Omega/\nu$ ($\Omega=2\pi F_{\mathrm{rot}}$ and ν is the fluid's kinematic viscosity) exceeds 10^5. The rms (root-mean-square) velocity fluctuation is $u_{\mathrm{rms}}\sim 4$ m/s and the Taylor micro scale is $\lambda\sim 1.3$ mm; this yields a turbulent Reynolds number $R_\lambda\sim 320$. We stress here that we only calculate an estimate of the turbulent Reynolds number R_λ; the Taylor micro scale is computed using $\lambda^2\sim 15\nu u_{\mathrm{rms}}^2/\epsilon$, where ϵ (the rate of energy dissipation per mass unit) is deduced from an independent measurement of the global power consumption of the flow.[31] The Kolmogorov length scale is of order $\eta\sim 30\,\mu$m.

Typical velocity and pressure data are shown in Fig. 2. One observes on the pressure signal—Fig. 2(b)—the characteristic drops that have been attributed to the sweeping of vorticity filaments over the probe.[10,11] On the velocity recordings—Fig. 2(a), one can already note the velocity increase associated to the pressure drops, and also that the signal is rectified—see the signals Probability Density Functions (PDF) shown in Figs. 2(c) and 2(d). The rectification is produced because the probe is located near the wall (2 mm from it) and is sensitive to the velocity modulus only. However, we note that it is mainly an effect of the slow large scale dynamics of the flow: when the velocity signal is high pass filtered with a cut-off frequency of 4 Hz, its PDF is more symmetric. The PDF of the increments for large lag τ are close to Gaussian, as it is usually observed. In addition, the skewness of the velocity increments behaves as usually observed in such intermediate Reynolds number flows: true scale invariance is not observed (see Sec. IV), but its value is in agreement with the measurement of the flow power consumption ϵ. Finally, we note that the power spectra of pressure and velocity display traditional Kolmogorov scaling ranges—Figs. 2(e) and 2(f).

III. COHERENT STRUCTURES: DETECTION AND ANALYSIS

A. Detection technique

In most cases, the identification of coherent structures in a 3D (three-dimensional) turbulent flow has been performed thanks to a detection of ''events'' on the velocity signal u. This was done by thresholding high-pass-filtered versions of u,[32] or thresholding its wavelet coefficients,[9] or using the so-called Wavelet Transform Modulus Maxima (WTMM) technique.[33] Here, we adopt a different point of view which relies on the measurement, joint in time and space, of the pressure p and the velocity u signals. As earlier explained, previous measurements in this geometry have shown that sudden pressure drops are produced by the passage of vorticity filaments over the transducer. Therefore, we identify vortices in u by detecting pressure drops in p; then, we perform a statistical analysis of u conditioned to p. Again, several methods have previously been proposed to detect the strong drops observed in turbulent pressure signals (thresholding technique,[34] WTMM,[35] wavelet-based thresholding method[7] $\cdots$). They have all shown that the strong observed depressions are responsible for the significant departure from Gaussianity of the probability density function of p [see Fig. 2(d)]. Previous experimental studies[7,34] showed that p is close to Gaussian if the drops are removed from the signal (we checked this property *a posteriori*). Therefore, we propose to design a pressure drop detector based on the measurement of large departures from Gaussianity, using the cumulants of the pressure data.

Let us recall that the cumulants of a centered process X are defined by

$$C_n = \left(\frac{d^n}{dq^n} \ln \langle e^{qX} \rangle \right) \Bigg|_{q=0}. \tag{1}$$

For instance:

$$\begin{aligned} &C_1 = \langle X \rangle = 0, \quad C_2 = \langle X^2 \rangle, \quad C_3 = \langle X^3 \rangle, \\ &C_4 = \langle X^4 \rangle - 3C_2^2 \cdots, \end{aligned} \tag{2}$$

where $\langle\ \rangle$ denotes the ensemble average. The Gaussian distribution is entirely determined by its two first cumulants; all its cumulants of order higher than two are equal to zero. In order to detect local departures from Gaussianity, we compute the local fourth-order cumulant $\hat{C}_4(k)$ from the time series $X(k)$. A recursive local estimator has been proposed in Refs. 36 and 37

$$\begin{cases} \hat{M}_2(0) = 0, \hat{C}_4(0) = 0 \\ \hat{M}_2(k) = \hat{M}_2(k-1) + \mu(X(k)^2 - \hat{M}_2(k-1)) \\ \hat{C}_4(k) = \hat{C}_4(k-1) + \gamma(X(k)^4 - 3X(k)^2 \hat{M}_2(k-1) \\ \qquad - \hat{C}_4(k-1)), \end{cases} \tag{3}$$

where $\hat{M}_2$ is an estimate of the second-order moment, k is the time position, and μ and γ are coefficients to be chosen. This estimator $\hat{C}_4(k)$ has to satisfy the usual trade-off: It has to be sensitive enough to detect close successive events (i.e., to avoid to miss detections) and it should not be too sensitive to avoid false alarm detections. The parameters μ and γ determine the characteristic length scale of the response of the detector $\hat{C}_4(k)$. Using synthetic numerical data reproducing as closely as possible the statistical characteristics of the p-signal, μ and γ are empirically set to $\mu = 0.0025, \gamma = 0.025$ which optimize the trade-off mentioned above. We have checked that the results presented below do not depend on these precise values. As shown in Fig. 3, the cumulant $\hat{C}_4(k)$ is zero almost everywhere except when a low pressure event is observed.

The detection algorithm consists of the two following steps. First we compute the running fourth order cumulant from the normalized pressure signal $(p - \bar{p})/p_{\mathrm{rms}}$; the normalization is necessary to apply the same procedure to signals with different p_{rms} values, i.e., flows at different Reynolds numbers. Then we detect the sequence k for which $\hat{C}_4(k) > 5$, the manually set thresholding value. Within a signal slab of fixed length Δ where a detection occurred, the precise instant k_i of occurrence of an event is defined as the time when $\hat{C}_4(k)$ is maximum. We request that the minimal time interval between successive detections be larger than $T_{\mathrm{rot}}/5$ where $T_{\mathrm{rot}} = 1/F_{\mathrm{rot}}$. This is consistent with previous work[11] which have shown that the mean waiting time between pressure drops is of order $10\,T_{\mathrm{rot}}$.

We also used a more standard thresholding detection technique as a comparison: Threshold $= -4.5 p_{\mathrm{rms}}$ (as used in previous work[11]) and $-3p_{\mathrm{rms}}$. The results obtained by using the cumulant method or the thresholding technique (threshold $= -3p_{\mathrm{rms}}$) are quasi identical for the detection lists themselves as well as for further general consequences. We stress that a detection of the (positive) peaks on $\hat{C}_4(k)$ is much easier than that of the (negative) ones on p. This is due to a weak level of noise in $\hat{C}_4(k)$ and it yields a precise localization of the time instants k_i where the drops occur. Finally, we have computed the histograms of the pressure signal on data series where the filaments signature only is kept (filaments) and for the rest of the pressure signal (background). The resulting PDFs are shown in Fig. 4 where a Gaussian is plotted for comparison. As expected it is clear that the detected events are responsible for most part of the exponential tail towards low pressures.

B. Statistics of the interarrivals

Figure 5 is obtained by drawing a vertical line at each instant of detection and shows that arrivals seem to form clusters. This should be apparent in the PDF of the interarrivals. From 100 lists of about 90 events each (8892 events exactly), we compute the PDF of the waiting times, shown in Fig. 6. The lin-log plot in Fig. 6(a) suggests that this PDF is well modeled by a Poisson law ($\sim \exp(-t/\tau)$, $\tau \sim 20 T_{\mathrm{rot}}$) for the long waiting times ($\Delta t > 15 T_{\mathrm{rot}}$), but also shows a clear departure from this Poisson law for the short waiting times. The log–log plot in Fig. 6 indicates that a power law ($\sim \Delta t^{-2}$) could well model this short waiting time part of the PDF. Note that this cutoff point is an order of magnitude greater than the integral time scale T_{rot}. Interestingly, let us recall that a Poisson law very often points to statistically

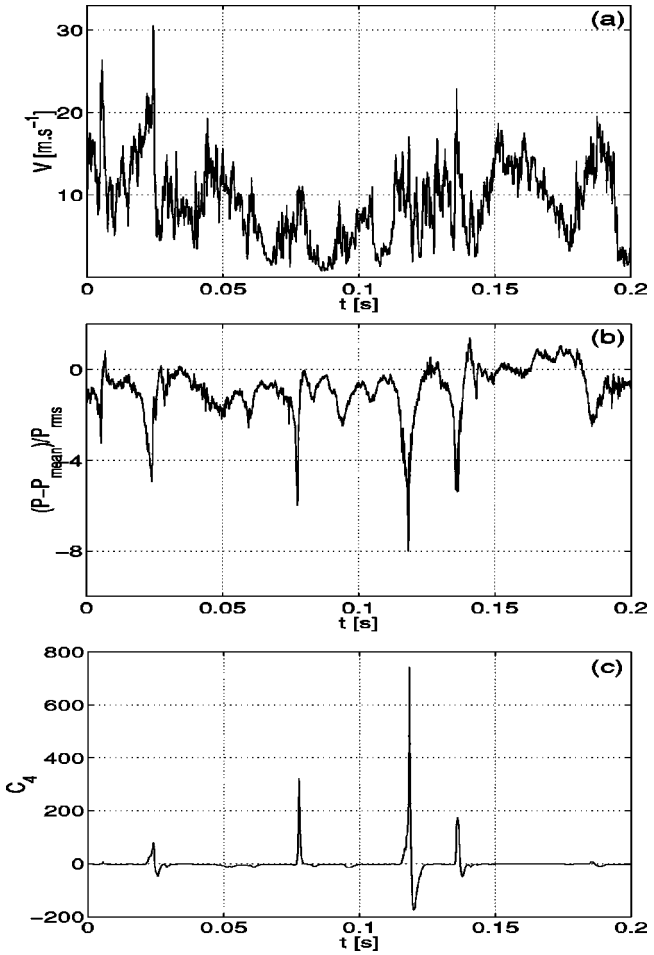

FIG. 3. Cumulant based detection. (a) velocity signal; (b) (centered and normalized) pressure signal; (c) sliding estimate of the fourth-order cumulant, performed on the pressure time series.

independent events. A power law for the PDF could be associated with a statistical correlation (see, e.g., Refs. 23 and 38). With such a picture in mind, the change point around $\Delta t \sim 15 T_{\mathrm{rot}}$ can therefore be understood as a maximum correlation duration within the interarrivals list. Events belonging to the same cluster in Fig. 5 would be correlated while different clusters would not. These results are similar to the ones reported in Refs. 7, 23 and 32 where a cutoff around $\Delta t \sim 10 T_{\mathrm{rot}}$ was observed. In Ref. 34 a departure from a Poisson law was observed for $\Delta t < T_{\mathrm{rot}}$. On the contrary, a pure Poisson law with no departure at short interarrivals was reported in Ref. 35 but on the basis of a different definition of the detected events.

C. Average velocity pattern

We compute the time signature related to the occurrence of pressure drops, both for the pressure and the velocity, by a synchronous averaging performed over slabs centered on the instants k_i of detection. The results are shown in Fig. 7. As expected, the average signature in p is a strong drop of about $-4p_{\mathrm{rms}}$: The cumulant method detects pressure drops. In addition, despite the fact that the detection is performed on p, a nontrivial pattern is observed in u. It indicates that the drops recorded on the pressure sensor can be associated with

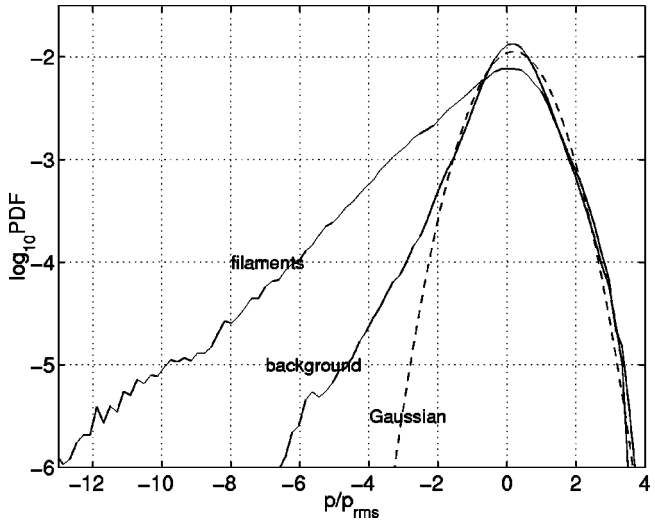

FIG. 4. Conditional PDFs of the pressure signal. The PDF of the part of the pressure signal corresponding to the filaments only is computed on windows of fixed size around the instants of detection; the PDF of the background is obtained from the remaining signal.

the existence of structures with a specific velocity profile in the turbulent flow. We have checked that averaging over a set of instants chosen at random gives a trivial signature.

According to experimental observations,[11,13,34,39,40] the average profiles are expected to correspond to the passage of a vorticity filament in the vicinity of the sensors. In the spirit of the analysis presented in Ref. 6, we model the effect of a filamentary vortex sweeping the pressure and velocity probes. For simplicity, we consider the case of a Burgers vortex although we make no claim on the actual structure of the vorticity filaments. The results presented hereafter do not crucially depend on this particular choice.

Let us first set some useful notations. For a straight Burgers' vortex aligned on the z axis and with vorticity $\omega(r) = \omega_0 e^{-\gamma r^2/4\nu}$, the velocity and pressure fields are given by

$$u_r = -\frac{1}{2}\gamma r, \quad u_\varphi = \frac{\Gamma}{2\pi r}(1 - e^{-(r/2r_0)^2}), \quad u_z = \gamma z, \quad (4)$$

$$p(r) = -\frac{\rho \Gamma^2}{4\pi^2 r_0^2} \int_{r/r_0}^{\infty} \frac{(1 - \exp(-x^2/4))^2}{x^3} dx, \quad (5)$$

where (x,y,z) and (r,ϕ,z) are rectangular and cylindrical coordinates, γ is the stretching rate of the vortex, $r_0 = \sqrt{\nu/\gamma}$ its characteristic radius and $\Gamma = \pi r_0^2 \omega_0$ its circulation. As the measurements are performed near the wall ($\sim$2

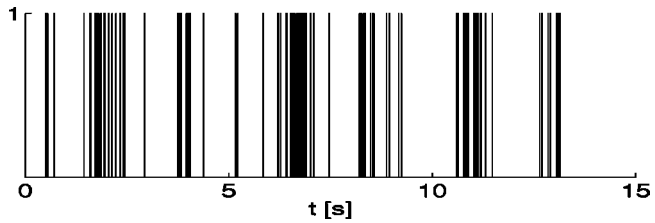

FIG. 5. Cumulant based detection list. A vertical solid line is drawn at each detection time. We observe that events are detected in clusters.

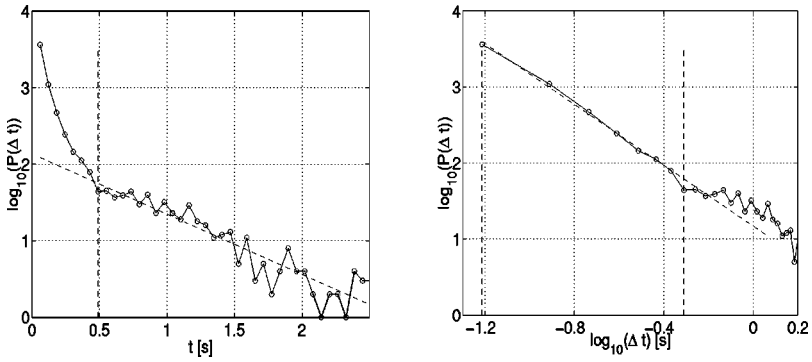

FIG. 6. Probability density functions of the waiting times between pressure drops. (left) lin–log plot: This PDF is well modeled by a Poisson law ($\sim\exp(-t/\tau)$, $\tau\sim 20\,T_{\rm rot}$) for the long waiting times ($\Delta t > 15T_{\rm rot}\sim 0.5$ s); (right) this log–log plot indicates that a power law ($\sim\Delta t^{-2}$) could well model the short waiting time part of the PDF.

to 3 mm), we consider in first approximation and in agreement with previous observations,[11,34] that the detected vortices are perpendicular to the wall and we neglect the axial velocity compared to the azimuthal one. Thus, for a vortex locally advected at velocity $\vec{U}$, at distance δ from the probe and in a direction making an angle α with the hot wire, one measures (see Fig. 8)

$$u_{\rm meas}(t)=\left|U\cos\alpha+u_{\varphi}(r)\frac{y}{r}\right|. \tag{6}$$

Different patterns can be obtained (see Fig. 9) depending on the choice of the parameters (U, max($|\Delta p|$), α, δ, and r_0) of the model. Some sets of parameters do not contribute to the average pattern: Those, for instance, that generate a symmetrical velocity signal such as in Fig. 9(b). Other sets, as in Figs. 9(a) or 9(c) contribute, on average, to a pattern shown in Fig. 9(d), which is quite similar to the experimentally observed time shape. This shows that the average velocity pattern is well represented by the case $\alpha=0$, as expected from the symmetry of the motion of the filaments about the Ox axis (the pressure probe is not sensitive to α). Next, we observe that the distance δ between the filament and the probe must be chosen in a finite range. On one hand, δ is necessarily nonzero ($\delta=0$ gives a zero-signature on u) so that it must be greater than, say, 0.1 mm. On the other hand, δ has to be smaller than $\delta_{\rm max}\sim 5$ mm, otherwise the drop would not be detected by the pressure probe. Eventually, δ must be in the interval [$\delta_{\rm min}\sim 0.1$ mm, $\delta_{\rm max}\sim 5$ mm] [see examples with different choices of δ in Figs. 10(a)–10(c)]. Next, we observe that U can be chosen as the average velocity $\bar{U}$ at the probe location and that the value of max($|\Delta P|$) can be directly deduced from the measurement. Hence, δ and r_0 remain the only free parameters. Figure 7 compares the experimentally observed velocity and pressure patterns (solid lines) with these of the Burgers model (dashed lines), for the best fit of parameters, $\delta=1.4$ mm and $r_0=3.2$ mm. The striking similitude between the experimental results and the analytical model together with previous observations allow us to associate the occurrence of pressure drops with the existence of coherent structures that exhibit a clear vortex signature in the turbulent flow. Moreover we can give an order of magnitude for the typical size of these vortex-filaments: Their typical radius is $r_0\sim 3$ mm, of the order of magnitude of the Taylor scale $\lambda\sim 1.3$ mm (whereas the radius of the smallest events that the pressure probe can detect is of order of 0.5 mm). This is consistent with earlier

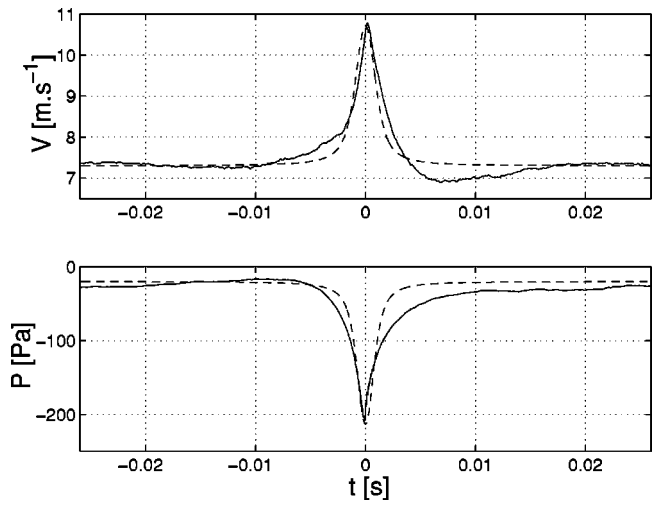

FIG. 7. Patterns of the coherent structures. The solid lines show the velocity (top) and pressure (bottom) patterns obtained by a conditional averaging performed at the instants where pressure drops occur. These patterns are compared to those obtained using Burgers' model (dashed lines). The parameters of the best fit for Burgers' model are: $U=V_{\rm mean}=7.3$ m.s^{-1}, max($|\Delta P|$)=max($|\Delta P_{\rm meas}|$)=200 Pa, $\alpha=0$, $\delta=1.4$ mm, $r_0=3.2$ mm.

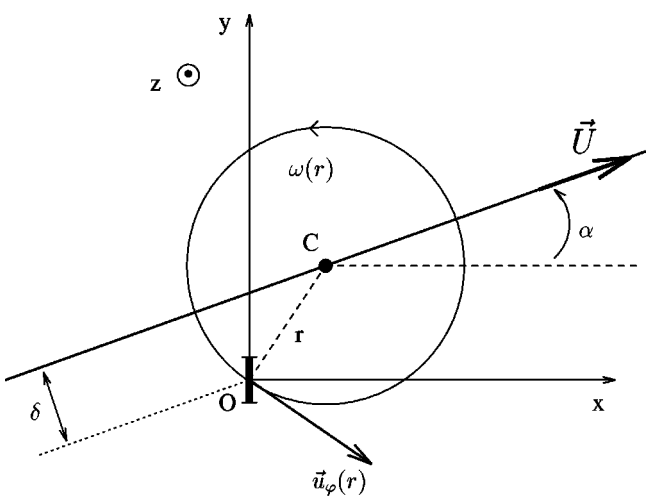

FIG. 8. Model description of a filamentary vortex motion over the hot wire probe. The wall is parallel to the (xOy) plane. The hot wire and pressure probes are located at the origin O. The vortex is aligned on the z axis and advected at velocity $\vec{U}$.

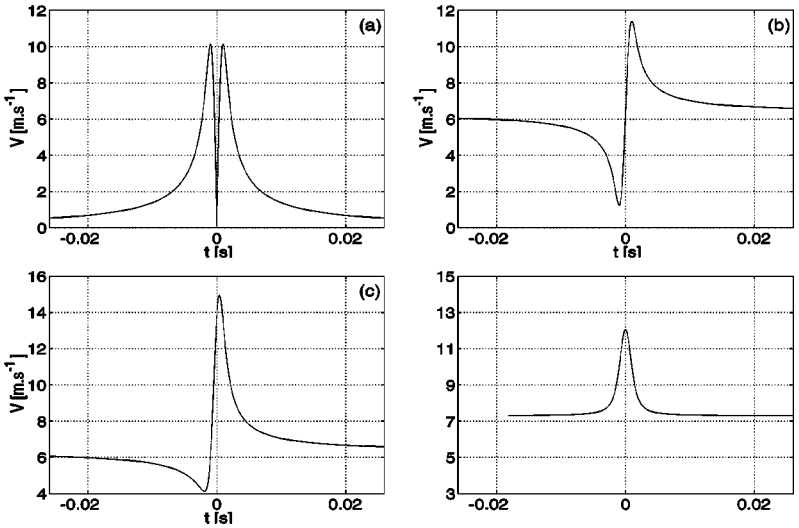

FIG. 9. Typical velocity patterns for the Burgers model. (a) $\alpha=\pi/2,\delta=0$; (b) $\alpha=\pi/6,\delta=0$; (c) $\alpha=\pi/6,\delta=3$ mm; (d) $\alpha=0$, $\delta=2$ mm.

findings[17,18,35,41] which showed that filamentary vortices have a statistical core size related to the Taylor microscale.

IV. INTERMITTENCY AND COHERENT STRUCTURES: A WAVELET ANALYSIS

In previous sections, we have detected coherent objects in the flow and we have studied their statistical characteristics. The purpose of this section is to investigate the connection between the existence of coherent objects in the flow and its intermittent nature. By intermittency we mean statistical departure from the exact self-similarity description of the velocity field, known as the Kolmogorov 41 theory. Actually we define intermittency as the variation of the PDFs of the velocity increments as the lag τ over which the increments are computed is varied. These deformations of the probability density functions are usually studied through the structure functions. In this section, we intend to compare the structure functions of the whole velocity signal to *conditional* structure functions, related to the *background* and *filament* phases. (The word ''phase'' is abusively used here, as filaments and background signal are not ''states'' of the turbulent velocity field, but portions of the signal selected by the pressure detector)

Computation of conditional structure functions has already been proposed. In Refs. 7,23 and 35, the structure functions of the whole pressure signal are compared to those related to background and filament phases, using a detection performed on the pressure signal itself. In Refs. 6 and 9, the structure functions of the entire velocity signal are compared to those related to a filament phase or a background phase, respectively, using detections performed on the velocity signal itself. Here, we propose to compare the structure functions of the complete velocity signal to these related to background and filament phases, using a detection procedure applied to the jointly recorded pressure signal. In addition, as motivated in the introduction, we will use wavelet-based structure functions instead of usual ones and, therefore, we first introduce them and note their main properties.

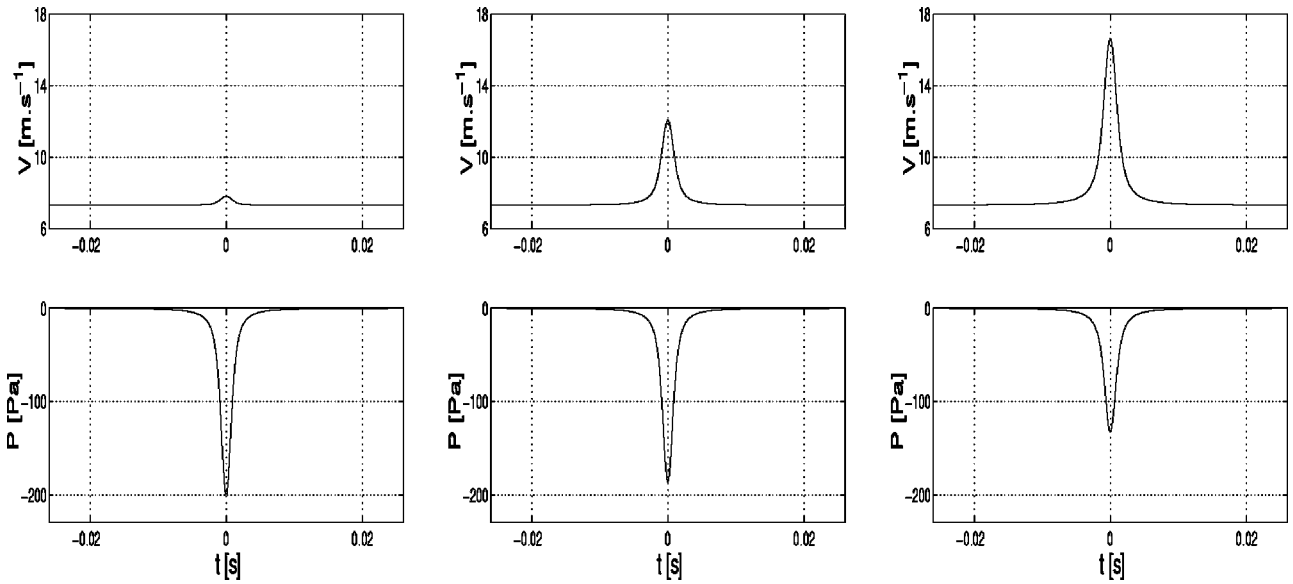

FIG. 10. Velocity and pressure patterns for the Burgers model. $\alpha=0$ and (left) $\delta=0.2$ mm, (middle) $\delta=2$ mm, (right) $\delta=5$ mm.

A. Wavelets and structure functions

The probability density functions of the increments are studied through their moments. Under common hypothesis of stationarity and ergodicity of the increments processes, the moments of the absolute values can be estimated using the so-called structure functions (SF)

$$S_q(\tau)=\int |X(t+\tau)-X(t)|^q d, \quad q>0, \tag{7}$$

where X is the process to be analyzed, and τ the lag. As is often done in the study of intermittency in fully developed turbulence,we confine ourselves to the study of the absolute values of the increments (and abusively use the term ''structure function''); this is necessary for the cascade formalism developed here, as will become apparent in the next subsection.

Classical assumptions, usually made in turbulence and understood as generalizations of Kolmogorov's pioneering analysis,[42] claim that within the inertial range, the SF follow a power law

$$S_q(\tau)\sim|\tau|^{\zeta_q}, \quad \tau_{\min}\leqslant\tau\leqslant\tau_{\max}, \tag{8}$$

and that the departure of the ζ_q exponents from a linear behavior traces back to intermittency. Indeed, the fact that the function ζ_q is linear in q ($\zeta_q=q/3\ \zeta_3$) implies that the PDFs of increments for various τ's would collapse together, under suitable renormalization depending on ζ_3 only. This would mean that the shapes of the PDFs of the increments are similar. On the contrary, the departure of the ζ_q exponents from a linear behavior describes how those PDFs are varying with τ and, therefore, traces back to the statistical intermittency as defined above.[43]

In this respect, the extended self-similarity (ESS) scheme[44] has become widespread in the analysis of scaling in turbulence. It consists in testing the scaling of the SFs, one against the other, instead of against the τ variable, i.e., $S_q(\tau)\sim S_p(\tau)^{\xi(q,p)}$. In the context of turbulence, because of the theoretical Kármán–Howarth equation,[45] $S_3(\tau)$ often plays a specific role and we define $\xi(q)\equiv\xi(q,3)$.

We now revisit the analysis of scaling in turbulence using wavelets. Let us first start with some definitions of the wavelet analysis. The coefficients $T_X(a,t)$ of the wavelet transform of a process X results from comparisons, by means of inner products, between the process to be analyzed X and a family of analyzing functions

$$T_X(a,t)=\langle X,\psi_{a,t}\rangle=\int X(s)\psi_{a,t}(s)ds. \tag{9}$$

The analyzing functions

$$\psi_{a,t}(s)=\frac{1}{a}\psi_0\left(\frac{s-t}{a}\right), \tag{10}$$

are dilated and translated templates of the mother-wavelet ψ_0. The time delay operator, $\psi_{0,t}(s)=\psi_0(s-t)$, allows to select the time position around which the analysis has to be made, while the dilation (or change of scale operator), $\psi_{a,0}(s)=1/a\,\psi_0(s/a)$, selects the length of the analyzing window (or equivalently the range of analyzed frequencies). Moreover the mother wavelet ψ_0 is characterized by its number of vanishing moments N such that

$$\forall k\in[0,1,\ldots,N-1], \quad \int t^k\psi_0(t)dt=0. \tag{11}$$

By definition of the wavelet transform, $N\geqslant 1$.[46] This parameter plays a key role in the analysis of scaling presented below (see also Refs. 25 and 26). We note that the more traditional increments can be exactly rewritten as wavelet coefficients, computed with the special example of wavelet: $\psi_0(t)=\delta(t+\tau_0)-\delta(t)$. Indeed, in this case

$$\begin{aligned}T_X(a,t)&=\int X(s)\left[\delta\left(\frac{s-t}{a}-\tau_0\right)-\delta\left(\frac{s-t}{a}\right)\right]\frac{ds}{a}\\&=X(t+\underbrace{a\tau_0}_{\tau})-X(t).\end{aligned} \tag{12}$$

Such a wavelet is poor because it is very irregular, has only one vanishing moment ($N=1$), and very low spectral localization.

Wavelet coefficients, therefore, constitute a powerful generalization of the increments with respect to regularity and spectral localization which ensure better statistical properties to study the data around a given time scale. Wavelet based structure functions (WSF) are defined as (see, e.g., Ref. 22)

$$S_q^{wt}(a)=\int |T_X(a,t)|^q dt, \tag{13}$$

and the wavelet counterpart of $S_q(\tau)\sim|\tau|^{\zeta_q}$, $\tau_{\min}\leqslant\tau\leqslant\tau_{\max}$ reads

$$S_q^{wt}(a)\sim a^{\zeta_q}, \quad a_{\min}\leqslant a\leqslant a_{\max}. \tag{14}$$

The ESS-ansatz applied to the WSF (see, e.g., Ref. 9) now reads

$$S_q^{wt}(a)\sim(S_p^{wt}(a))^{\xi^{wt}(q,p)}. \tag{15}$$

For simplicity, we again write $\xi_q^{wt}\equiv\xi^{wt}(q,3)$. The relation between the (wavelet-)ESS, cascade models and the existence of coherent structures in turbulent flows will be a key point of our experimental study in the next subsection.

From a technical point of view, let us note that we replace the usual definition $\psi_{a,0}(s)=1/\sqrt{a}\,\psi_0(s/a)$ by $\psi_{a,0}(s)=1/a\,\psi_0(s/a)$. While the former choice insures energy conservation of the analyzing functions, the latter better suits scaling behaviors analysis; for example, it reproduces exactly the Hölder regularity of a process.[47] Moreover, instead of using the Continuous Wavelet Transform (CWT) $T_X(a,t)$ defined above, we perform a Discrete Wavelet Transform (DWT)[47,46] which amounts to computing the wavelet coefficients on a specific set of points called the dyadic grid

$$d_X(j,k)=T_X(a=2^j,t=2^jk). \tag{16}$$

In the DWT framework, the WSF are written as[25]

$$S_q^{wt}(a=2^j)=\frac{1}{n_j}\sum_k |d_X(j,k)|^q, \tag{17}$$

where n_j is the number of available coefficients at each octave j (or equivalently each scale 2^j). To simplify notations, we abusively write: $S_q^{wt}(j) \equiv S_q^{wt}(a=2^j)$. In the scaling range, one has:[48] $S_q^{wt}(2^j) \sim 2^{j\zeta_q}$. The coefficients of the DWT can be efficiently computed using the fast pyramidal recursive algorithm, known as Mallat's algorithm.[47] Note that such an algorithm computes wavelet coefficients defined using the energy conservation normalization.

The wavelet decomposition is basically a joint time-frequency analysis of the data, which means that the coefficient $d_X(j,k)$ contains information on X located around time $t=2^jk$ and scale 2^j. This allows to compute WSF that are conditioned to partitions of the time-frequency contents of the data. Here we use it to compute the structure functions related to the filament and background phases. To wit, we perform a DWT on the velocity signal and separate the wavelet coefficients $d_X(j,k)$ into two phases: The filaments and the background. Let k_i be the time positions where detections are performed. The wavelet coefficients corresponding to the filament phase are such that (j,k) satisfy $k_i - \Delta/2 < 2^jk < k_i + \Delta/2$ (Δ is the length of the slab, cf. Sec. III A) and are labeled $d_X^{(f)}(j,k)$. The remainder of the $d_X(j,k)$ belong to the background phase and are labeled $d_X^{(b)}(j,k)$. We compute the following three WSF:

$$S_q^{wt}(j) = \frac{1}{n_j} \sum_k |d_X(j,k)|^q,$$

$$S_q^{wt,(f)}(j) = \frac{1}{n_j(f)} \sum_k |d_X^{(f)}(j,k)|^q, \tag{18}$$

$$S_q^{wt,(b)}(j) = \frac{1}{n_j(b)} \sum_k |d_X^{(b)}(j,k)|^q,$$

where $n_j(f)$ and $n_j(b)$ are the numbers of wavelet coefficients at octave j in the filament and the background phases.

B. Log-infinitely divisible cascade and wavelets

In the experimental analysis developed below, we study the scaling properties of turbulent data using a log-infinitely divisible cascade model. It belongs to the large category of models that describe scaling in data by means of multiplicative cascades[49,50] and was introduced in the form described here by Castaing.[51] We briefly resketch it and rewrite it in the wavelet framework.

The description of the turbulent cascade relies on the use of the following functional equation to describe the evolution with l of the PDF P_l of the velocity increments $\delta u(l) = u(t+l) - u(t)$

$$\forall l \quad \text{and} \quad l', \quad l \leqslant l',$$

$$P_l(\ln|\delta u(l)|) = \int G_{ll'}(\ln\alpha) P_{l'}(\ln|\delta u(l)| - \ln\alpha) \frac{d\ln\alpha}{\alpha}, \tag{19}$$

where $G_{ll'}$ is the so called *propagator*, which only depends on l and l'. Physically, the above equation means that the PDFs of velocity increments can be continuously deformed, from the integral scale to the dissipative one. Note that this analysis implies the use of absolute values for the increments.

The Laplace transform of this equation with respect to the variable $\ln|\delta u(l)|$ yields

$$\langle |\delta u(l)|^q \rangle = \hat{G}_{ll'}(q) \langle |\delta u(l')|^q \rangle, \tag{20}$$

where $\hat{G}_{ll'}(q)$ is the Laplace transform of $G_{ll'}(\ln\alpha)$, which fully characterizes the multiplicative cascade of the velocity increments $|\delta u|$.

This cascade is said to be *log-infinitely divisible* or *continuously self-similar* if there exist two functions $\hat{G}(q)$ and $n(l)$ such that

$$\hat{G}_{ll'}(q) = [\hat{G}(q)]^{n(l)-n(l')}, \tag{21}$$

In this formulation, $\hat{G}(q)$ describes the elementary step of the cascade, while $n(l)$ determines its scale dependence. In other words, $\hat{G}(q)$ defines the basic element or the basic operation controlling the PDF deformation, while $n(l) - n(l')$ defines the number of times $\hat{G}(q)$ is to be applied to cascade from scale l' to scale l. In some sense, $dn(l)/d(l)$ [or equivalently, $dn(l)/d\ln(l)$] represents the ''speed'' of deformation of the PDF as a function of the scale. Obviously, this splitting of $\hat{G}_{ll'}(q)$ into separable functions of q and l is not unique and implies some arbitrary choices of reference. This will be discussed in the data analysis section so as to make comparisons meaningful.

By definition, the cascade is said to be *scale invariant* if

$$n(l) - n(l') = \ln(l) - \ln(l') = \ln(l/l'). \tag{22}$$

Note that in this case, it is the logarithmic function that makes $n(l) - n(l')$ a function of l/l' only; this does not need to be always the case and should rather be seen as an exception. In general one would need a reference scale l_0.

Continuing the analogy between increments $\delta u(l)$ and wavelet coefficients $d_X(j,k)$ one can extend the log-infinitely divisible cascade definition to wavelet-based structure functions.[52] Keeping in mind that we want to test each phase separately, this amounts to write

$$P_a^{(\phi)}(\ln|T_X^{(\phi)}|) = \int G_{a,a'}^{(\phi)}(\ln\alpha) P_{a'}^{(\phi)}(\ln|T_X^{(\phi)}| - \ln\alpha) d\ln\alpha/\alpha,$$

$$\langle |T_X^{(\phi)}(a,t)|^q \rangle = \hat{G}_{a,a'}^{(\phi)}(q) \langle |T_X^{(\phi)}(a',t)|^q \rangle, \tag{23}$$

$$\hat{G}_{a,a'}^{(\phi)}(q) = [\hat{G}^{(\phi)}(q)]^{n^{(\phi)}(a) - n^{(\phi)}(a')},$$

where $^{(\phi)}$ denotes the considered phase, entire signal, background (b) or filaments (f). We write $H^{(\phi)}(q) = \ln \hat{G}^{(\phi)}(q)$ and let a' be an arbitrary constant reference scale; then combining the above equations, one obtains

$$\ln\langle |T_X^{(\phi)}(a,t)|^q \rangle = H^{(\phi)}(q) n^{(\phi)}(a) + C_{q,a'}^{wt(\phi)}, \tag{24}$$

which is the form that has to be tested in order to show that the log-infinitely divisible cascade model is correct. Note that Eq. (24) implies

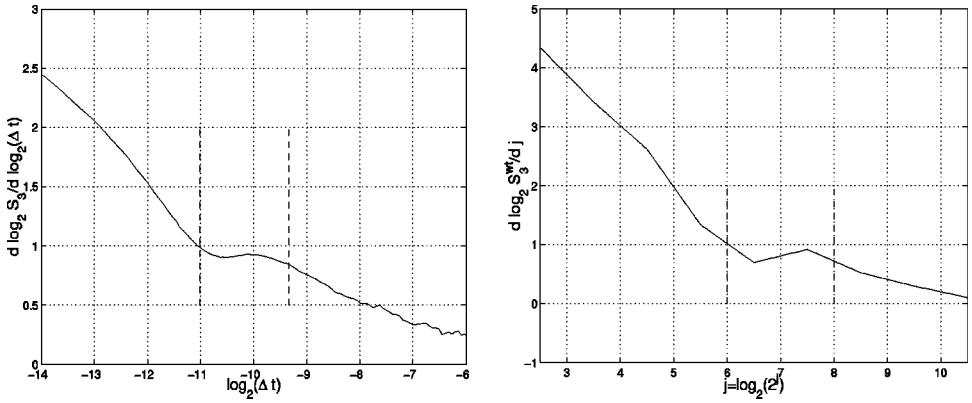

FIG. 11. Inertial range. Derivative of the logarithm of the classical third-order structure function (left) and derivative of the logarithm of the wavelet third-order structure functions (right). The vertical dashed lines show the supposed inertial range.

$$\ln\langle|T_X^{(\phi)}(a,t)|^q\rangle = \frac{H^{(\phi)}(q)}{H^{(\phi)}(p)}\ln\langle|T_X^{(\phi)}(a,t)|^p\rangle + \beta_{q,p,a'}^{wt(\phi)}, \tag{25}$$

which shows that the ESS property is fulfilled in the case of a log-infinitely divisible cascade. The fact that $\ln S_q$ is a linear function of $\ln S_p$ can be understood as a direct consequence of the log-infinitely divisible model. From the estimation of the slope in the $\ln S_q$ vs $\ln S_p$, one gets an estimate of H through $\xi^{wt(\phi)}(q,p)=H(q)/H(p)$. The main advantage of the log-infinitely divisible cascade formalism is that it allows to test both the *kernel* of the cascade (H) and its *development along the scales* (n).

C. Intermittency and filaments

1. Study of scale invariance

In a classical analysis of intermittency, a crucial issue is the estimation of the exponents ζ_q and the determination of their behavior as a function of q. The procedures used to estimate the exponents are identical in the SF and WSF cases. They consist in measuring the slopes of linear fits in log–log plots, namely a $\log S_q(\tau)$ vs $\log\tau$ plot gives $\hat{\zeta}_q$ for the SF, while a $\log_2 S_q^{wt}(j)$ vs $\log_2 2^j = j$ plot gives $\hat{\zeta}_q^{wt}$ for the WSF.

As it has been widely observed in ordinary turbulence, one major problem is that pure scaling laws do not strictly exist at moderate Re. One then needs a criterion to define the scaling domain (inertial range). We arbitrarily choose the regions where the velocity spectrum, the third-order structure function and the third-order wavelet structure function independently and satisfyingly obey a power law. This is not an absolute objective criterion to select a range of scaling but it is consistent with usual methods. In our experiments, we obtain for the wavelet (see Fig. 11):

$$j\in[j_1=6, j_2=8], \tag{26}$$

and, for the increments

$$\tau\in[\sim 0.49 \text{ ms}, \sim 1.5 \text{ ms}],$$

i.e.,

$$r\in[\sim 80\eta, \sim 250\eta]. \tag{27}$$

Note that if there is a quite clear way to establish a correspondence between a range of scales (as defined in the wavelet transform by a dilation factor) and a range of frequencies (as defined when using the Fourier transform), the connection with a range of lags for the increments remains only qualitative. We emphasize the fact that the results described below are in no way crucially dependent on these choices. Therefore, from now on, we keep these ranges unchanged and intend to compare estimates computed with the SF against those estimated with the WSF, varying the number of vanishing moments.

Scaling exponents have been measured from the SF and WSF using wavelets with $N=1,2,\ldots,7$ (namely the Daubechies compact support orthonormal wavelets, see Ref. 46). Table I compares these estimates (only $N=3,5,7$ are reported) and give 95% confidence interval for the wavelet estimates.

We note that the wavelet-based exponents are systematically smaller than the increment-based ones. This may result from the difficulty in defining a precise correspondence between the ranges of times (lag τ) and the ranges of scales (dilation factor a). In addition, we observe a dependence of the estimated exponents with the four chosen wavelets (recall that we understand the increments as a special case of wavelet coefficients), even though the estimates almost fall within error bars. Whereas the closeness of these estimated values guarantee that no artifacts like superimposed deterministic trends or nonscaling noises are corrupting the data,[53] it tends to show that the scaling behaviors within the inertial range are not rigorously exact[26] but may be regarded as relevant approximations (as is generally thought in turbulence). Lastly, we observe that the third-order exponent $\zeta_3 \sim 0.92$

TABLE I. Structure function exponents: ζ_q and ζ_q^{wt} estimated from the SF and WSF, for three different wavelets. The last column gives the 95% confidence intervals for the wavelet based estimates.

q	ζ_q	ζ_q^{wt} $N=3$	ζ_q^{wt} $N=5$	ζ_q^{wt} $N=7$	Conf. Int. (WT)
1	0.34	0.29	0.29	0.29	±0.01
2	0.64	0.56	0.55	0.56	±0.02
3	0.92	0.79	0.79	0.81	±0.02
4	1.15	0.99	0.99	1.03	±0.03
5	1.35	1.15	1.15	1.22	±0.04
6	1.49	1.24	1.25	1.37	±0.06
7	1.59	1.26	1.29	1.47	±0.08

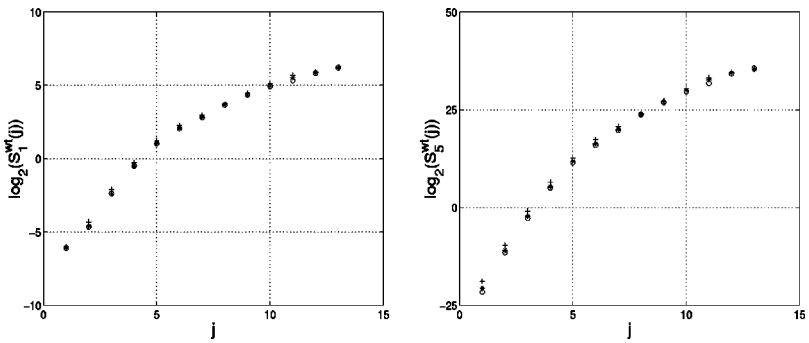

FIG. 12. Wavelet-based structure functions. $\log_2(S_1^{wt})$ (left) and $\log_2(S_5^{wt})$ (right) versus octaves j for the signal (*), the background (○), and filament (+) phases.

estimated from the classical SF is smaller than 1. When absolute values are used to compute the third-order moment, the value ζ_3 does not need to be constrained by the von Kármán–Howarth relationship (which may not be fulfilled since the measurements are made close to a wall). In addition, we note that similar lower values have been reported in experimental[20] and numerical[54] investigations of anisotropic, inhomogeneous flows.

We now measure the exponents ζ_q^{wt}, $\zeta_q^{wt,(f)}$, and $\zeta_q^{wt,(b)}$, corresponding, respectively, to the entire velocity signal and to its filament and background phases (with wavelet $N=7$ and for the fixed range $[j_1=6, j_2=8]$). These values are obtained separately from the conditional WSF computed as described in Sec. IV A. Examples of the WSF for each phase are shown in Fig. 12. We observe that the three curves look very much alike. Therefore, if it is possible to define tangency lines (and thus scaling exponents) for the entire velocity signal, then it is equally valid for the three phases. Again in each case a slight dependence with N for the $\zeta_q^{wt,(f)}$ and the $\zeta_q^{wt,(b)}$ is observed and is of the same order as that of the ζ_q^{wt}.

A careful examination of the WSFs reveals interesting changes in the estimated exponents. To wit, Table II gives the measured scaling exponents and their confidence intervals (also plotted as functions of q on Fig. 13). One observes that the exponents $\zeta_q^{wt,(b)}$, related to the background phase, are larger than the ζ_q^{wt} corresponding to the entire signal, themselves larger than the $\zeta_q^{wt,(f)}$ related to the filament phase. We emphasize the facts that (i) the differences between the estimated exponents for the three phases can be made quantitative: They do not fall within confidence intervals one of the other, and therefore, they cannot be considered as statistically identical (we recall that confidence intervals are theoretical ones computed by using the statistical properties of the wavelet transform[25]); (ii) the differences between the estimated exponents for the three phases are an order of magnitude larger than those, within a given phase, resulting from the variation of N. We, therefore, claim that the observed differences for the exponents ζ_q of the three phases are significant. In addition, we note a curvature effect: The $\zeta_q^{wt,(b)}$ curve is closer to a straight line than the ζ_q^{wt} one, and the $\zeta_q^{wt,(f)}$ is more rounded. The global effect (the exponents in the background phase have a more linear behavior than the exponents of the entire signal, and the exponents in the filament phase show more deviations from linearity) is significant without doubt. We have checked that these observations are robust against changes of the number N of vanishing moments and also against slight variations of the chosen bounds for the scaling region.

These results are consistent with a previously reported study[6] where the ζ_q exponents where shown to vary when conditioned to the presence of vorticity worms . However, in this case the detection and conditioning technique were quite different. Other investigations have also reported similar variations in the vicinity of a strong coherent vortex structure.[20,55]

From such an analysis, one may be tempted to conclude that the background phase tends to obey the K41 description of turbulence while the filament phase significantly departs

TABLE II. Conditional wavelet based structure functions exponents. This table is obtained with a Daubechies 7 (i.e., $N=7$) wavelet in the range $(j_1, j_2)=(6,8)$.

q	Signal	Background	Filaments
1	0.29±0.01	0.31±0.01	0.22±0.02
2	0.56±0.01	0.59±0.02	0.41±0.03
3	0.81±0.02	0.87±0.02	0.57±0.05
4	1.03±0.03	1.14±0.03	0.70±0.07
5	1.22±0.04	1.39±0.04	0.80±0.10
6	1.37±0.06	1.62±0.06	0.85±0.14
7	1.47±0.08	1.85±0.08	0.87±0.19

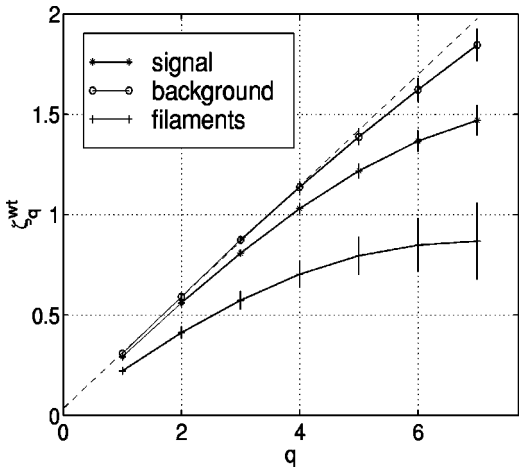

FIG. 13. Exponents of the wavelet based structure functions for the whole signal and the filament and background phases as a function of q. The dashed straight line is given as a linear reference.

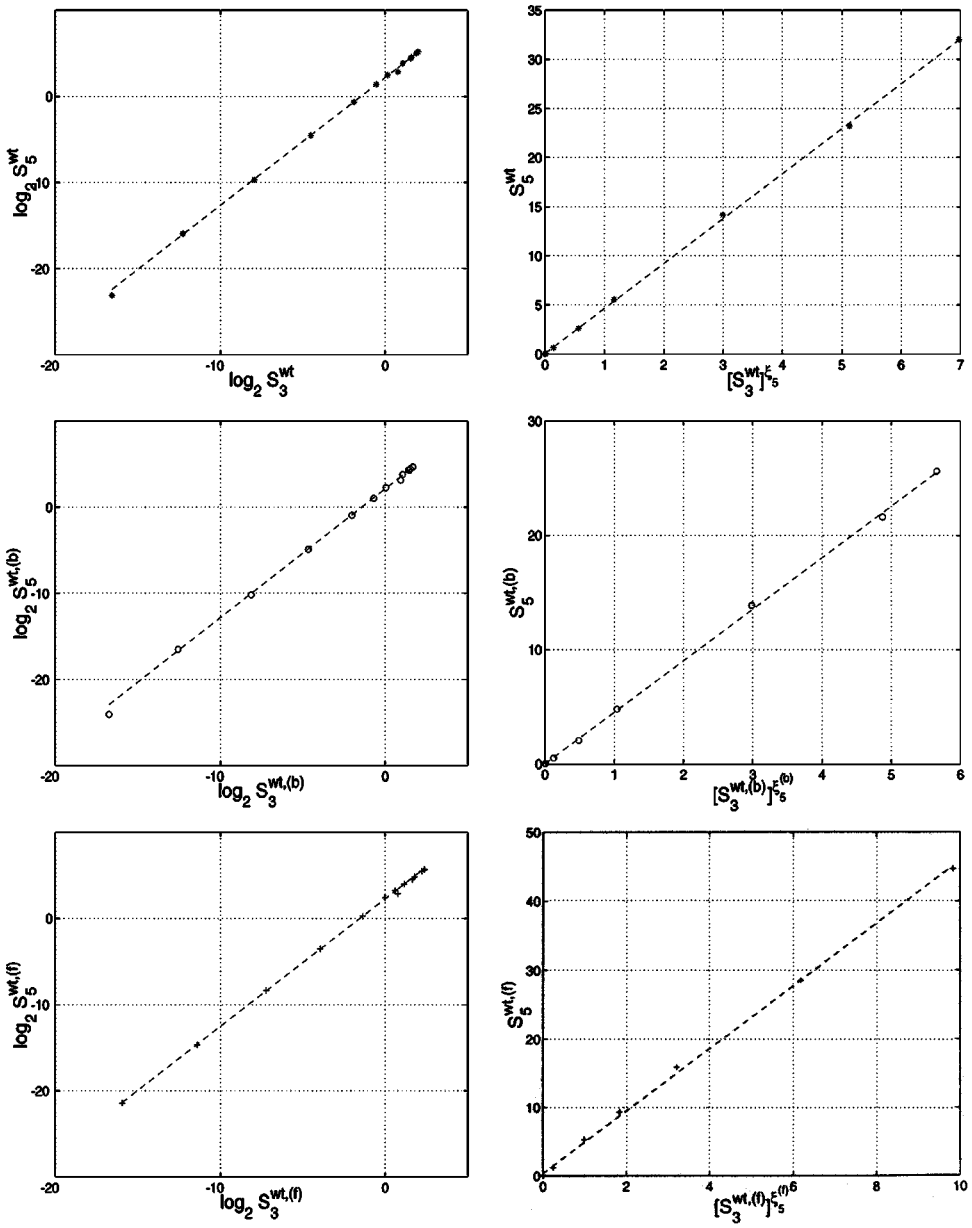

FIG. 14. Examples of extended self-similarity plots of the wavelet based structure functions for the three phases: (left) $\log S_5^{wt(\phi)}$ vs $\log S_3^{wt(\phi)}$ and (right) lin–lin plot of $S_5^{wt(\phi)}$ vs $(S_3^{wt(\phi)})^{\xi_5^{(\phi)}}$ for the different phases (ϕ): (top) whole signal, (middle) background phase, (bottom) filament phase. Note that the scaling $\xi^{wt,(\phi)}(5,3)=\frac{5}{3}$ that is expected at the finest scales is not observed due to lack of resolution in the dissipative range.

from it. Thus, the filaments would be responsible for statistical intermittency. We will show below by using a log-infinitely divisible cascade model how and why such an interpretation can be misleading.

2. Cascade analysis and extended self-similarity

In order to test the log-infinitely divisible model, we now plot $\log S_q^{wt(\phi)}$ vs $\log S_p^{wt(\phi)}$—see Fig. 14. We observe that the calculated points are well aligned on straight lines for all pairs (p,q) and for each of the three phases independently. This means that the ESS hypothesis is verified, so that one can write

$$\forall \phi, \quad \forall p,q, \tag{28}$$

$$\ln S_q^{wt(\phi)}(a)=\xi^{wt(\phi)}(q,p)\ln S_p^{wt(\phi)}(a)+\kappa_{q,p}^{(\phi)}.$$

If we further remark that $S_q^{wt(\phi)}(a)$ is an estimator of $\langle |T_X(a,t)|^q \rangle$, then Eq. (28) has clearly the same form as that of Eq. (25). Therefore, one can rewrite it as

$$\ln S_q^{wt(\phi)}(a)=H^{(\phi)}(q)n^{(\phi)}(a)+C_{q,p}^{(\phi)}, \tag{29}$$

and use it to estimate both the functions $H^{(\phi)}(q)$ and $n^{(\phi)}(a)$. Since their definitions imply the choice of a multiplicative constant, we set arbitrarily $H^{(\phi)}(3)=1$.

To study $H^{(\phi)}$, we estimate the slopes of the ESS plots (Fig. 14) and compute

$$H^{(\phi)}(q)=H^{(\phi)}(3)\xi^{wt(\phi)}(q,3)=\xi^{wt(\phi)}(q). \tag{30}$$

TABLE III. Extended self-similarity exponents $\xi_q^{wt,(\phi)}=\xi^{(\phi)}(q,3)$ of the wavelet based structure functions. Slopes of the $\ln S_q^{wt}$ vs $\ln S_3^{wt}$ plots, obtained with a *Daubechies 7* (i.e., $N=7$) wavelet in the range $(j_1,j_2)=(2,10)$ for the whole signal, the background and the filament phases separately.

q	Signal	Background	Filaments
1	0.39	0.39	0.40
2	0.72	0.71	0.72
3	⋯	⋯	⋯
4	1.25	1.26	1.25
5	1.48	1.50	1.48
6	1.69	1.70	1.70
7	1.88	1.89	1.91

The result is shown in Table III and Fig. 15. We observe that the exponents for the three phases are identical within experimental error. Hence $H^{(\phi)}$ does not depend on the phase (ϕ).

To study $n^{(\phi)}(a)$, we use the following procedure, based on relation (29):

(1) the functions $H^{(\phi)}(q)$ are those previously calculated;

(2) the constants $C_{q,p}^{(\phi)}$ appearing in Eq. (29), are determined by the arbitrary choice $C_{3,3}^{(\phi)}=0$ and calculated as

$$\ln S_q^{wt(\phi)}(a)-H^{(\phi)}(q)\ln S_3^{wt(\phi)}(a). \tag{31}$$

We have checked that the obtained value is independent of the scale a.

(3) For each q, an estimate of $n(a)$ can be computed as:

$$n_q^{(\phi)}(a)=(\ln S_q^{wt(\phi)}(a)-C_{q,3}^{(\phi)})/H^{(\phi)}(q). \tag{32}$$

We observe that the estimated functions $n_q^{(\phi)}(a)$ exhibit almost no dependence with q. Note that any dependence left could be *a posteriori* eliminated by an affine transformation $n_q'(a)=\alpha_q n_q(a)+\beta_q$: Indeed $\beta_q\neq 0$ is equivalent to a change in the value of the constant C_q, and $\alpha_q\neq 1$ is equivalent to replace the estimated value of $H(q)$ by $H(q)/\alpha_q$. As a result, a unique function $n^{(\phi)}(a)=\mathrm{mean}_q\{n_q^{(\phi)}(a)\}$ is determined for each phase. Together with the computation of $H^{(\phi)}(q)$, this shows that Eq. (29) and log-infinitely divisible cascades are valid models to describe the wavelet coefficients of the turbulence signal, independently for each phase.

The functions $n^{(\phi)}(a)$ are plotted in Fig. 16 (left). The first results are that the three $n^{(\phi)}(a)$ curves look globally

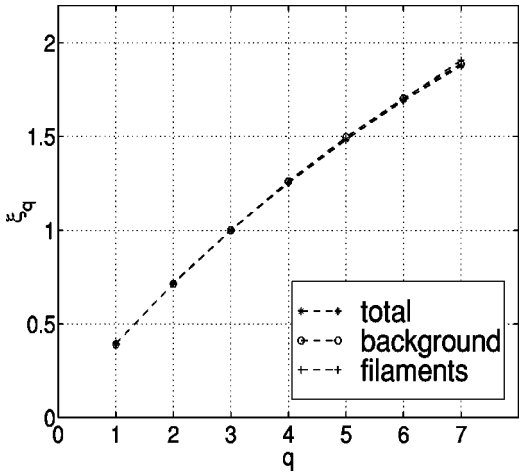

FIG. 15. Wavelet based structure functions relative exponents $\xi_q^{wt,(\phi)}$ for the three phases. The estimates are obtained using the wavelet *Daubechies7* $(N=7)$, within the range $(j_1,j_2)=(2,10)$.

similar and that they clearly cannot be modeled by $n^{(\phi)}(a)\propto\ln(a)$ over a significant range of scales. This means that the cascade in turbulence is not scale invariant. This is consistent with numerous observations at moderate Reynolds numbers, even in the case of isotropic homogeneous flows, and it is commonly accepted nowadays in the analysis of turbulence. Our analysis extends this to the background and filament phases. Instead of trying to approximate a limited (inertial range) part of the $n^{(\phi)}(a)$ curve, many attempts have been proposed to model a larger portion of $n^{(\phi)}(a)$, with the requirement that in the limit of infinite Re one should recover a logarithmic behavior. For instance, in Refs. 52 and 56, the following functional form has been proposed:

$$n_{\mathrm{approx}}(a)=\mu_1\frac{1-a^{-\beta}}{\beta}+\mu_2, \tag{33}$$

where the parameters μ_1, μ_2, and β may depend on the geometrical features of the flow and on the Reynolds number. Note that this form verifies $\lim_{\beta\to 0}[1-a^{-\beta}/\beta)]=\ln a$. Figure 16 (right) shows a comparison of our data with this form, using $\beta\sim 0.55$. This value is consistent with the ones reported in Ref. 56, where they also show the tendency of β to decrease as the Reynolds number increases.

Despite global resemblance between the three $n^{(\phi)}(a)$ functions, one observes (Fig. 17, left plot) clear differences

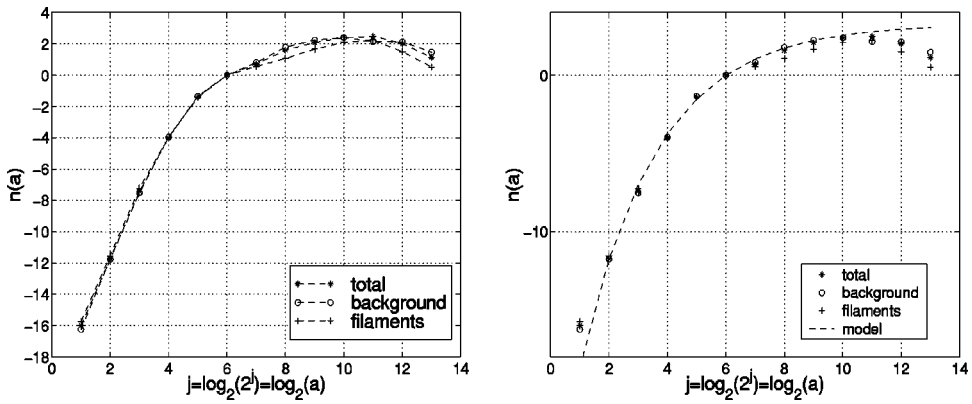

FIG. 16. Estimated functions $n^{(\phi)}$ (a). Left: $n(j)$, $n^{(b)}(j)$, and $n^{(f)}(j)$ estimated using the procedure described in the text; the scale $a'=2^6$ (octave $j=6$) was chosen as the reference (i.e., $n^{(\phi)}(2^6)=0$). Right: Modeling $n(a)$; $n(a)$ is compared to the model $n_{\mathrm{approx}}=17.71\ [(1-a^{-0.55})\ /0.55]-28.93$ (dashed line).

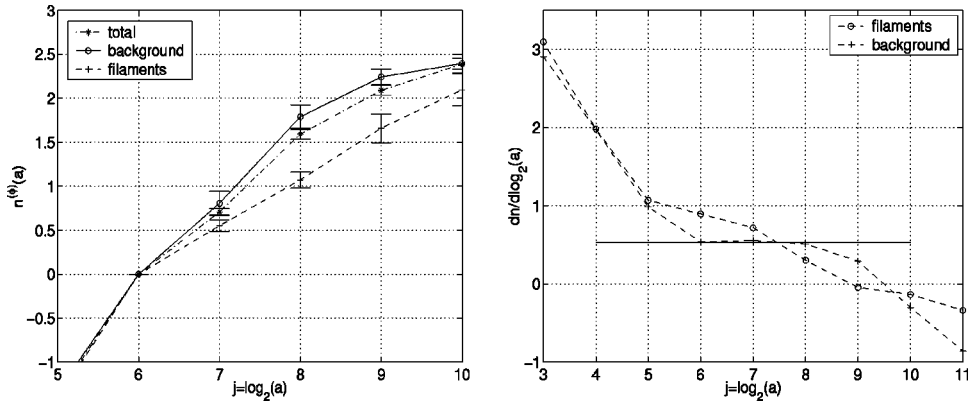

FIG. 17. Left: zoom on $n(a)$ in the range $(j_1,j_2)=(5,10)$. Right: $dn/d\log_2 a$ for the background and filament phases.

in the range of scales $[2^6,2^{10}]$, identified above as the inertial range. The error bars in this figure—they are experimental ones and result from the computation procedure described above—show that the curves cannot be considered as identical and that the differences are significant.

Such differences are consistent with the ones previously observed on the $\zeta_q^{wt(\phi)}$. Indeed these exponents were calculated as inertial range slopes

$$\zeta_q^{wt(\phi)}=\left.\frac{d\ln S_q^{wt(\phi)}(a)}{d\ln a}\right|_{\text{inertial range}} =H(q)\left.\frac{dn^{(\phi)}(a)}{d\ln a}\right|_{\text{inertial range}}. \tag{34}$$

Since the $H^{(\phi)}(q)$ are identical for all the phases, the phase dependence of the $\zeta_q^{wt(\phi)}$, which was explained to be significant in previous section, is related to the phase dependence of $dn^{(\phi)}(a)/d\ln a$. If we concentrate on the inertial range, Fig. 17 (left) suggests that the function $n^{(f)}(a)$ is closer to $\ln a$ than $n^{(b)}(a)$. This is clearly confirmed by Fig. 17 (right), which shows that $dn^{(\phi)}(a)/d\ln a|_{\text{decreasing}}$ is close to a constant for the filament phase, while increasing continuously for the two others. Therefore, it seems that the scale invariant assumption is better satisfied within the inertial range by the filament phase.

The experimental findings of this section are the following. Beyond the fact that ESS is satisfied, we show that the infinitely divisible cascade model is a valid description of turbulence, equally for the three phases. None of the cascade, however, is scale invariant over the range of available scales. While the $H^{(\phi)}(q)$ functions are identical for the three phases, the functions $n^{(\phi)}(a)$ significantly differ within the inertial range. It seems that the filament phase is closer to scale invariance ($n(a)\propto\ln a$) than the two others.

D. Discussion

We now return to the question of the relation between the existence of filament-type coherent structures in the flow and statistical intermittency.

A first experimental result is that a log-infinitely divisible cascade model describes the three phases equally well: Entire velocity signal, filament, and background phases. This suggests that this is a feature intrinsic to turbulence and not due to the filaments (at least in this set up).

A second experimental result is that the filaments act on the development of the log-infinitely divisible cascade. While the function $H(q)$ is not sensitive to filaments, the function $n(a)$ is. From the understanding of the role of these functions in the cascade described in Sec. IV B, we can say that, since the functions $H^{(\phi)}(q)$ are identical, the elementary deformation block $\hat{G}$ of the cascade is not controlled by the filaments. In the ESS analysis, this is equivalent to say that the relative exponents $\xi^{(\phi)}(q)$ do not depend on the presence of filaments. This conclusion seems to be in contradiction with that of a recent paper[57] where a phase sensitivity of H is reported. Note that the question of the universality of $H(q)$ versus experimental setup and Reynolds number—and hence of the ESS exponents—is still debated[58–62] and out of the scope of this paper. Back to the description of the cascade, the phase dependence of $n^{(\phi)}(a)$ indicates that the way the cascade proceeds along the scales depends on the presence of filamentary structures. Therefore, filaments do have an influence on turbulence intermittency. They act on the way the cascade develops along the scales but not on the way it is designed.

A third observation is that the ζ_q's are confusing quantities if one is to study intermittency at finite Reynolds number. We have shown that the $\zeta_q^{(\phi)}$'s significantly differ for the three phases and that the $\zeta_q^{(f)}$ are much farther from the linear behavior in q than the $\zeta_q^{(b)}$. From these results, two conclusions might be drawn. One is that the filaments do influence intermittency. Another is that the filament phase is *more* intermittent than the background one so that the latter is closer to the Kolmogorov 41 model. As shown using the more refined log-infinitely divisible cascade model, the first conclusion is correct (though inaccurate) while the second is not. Through the relations

$$\zeta_q^{wt(\phi)}=\left.\frac{d\ln S_q^{wt(\phi)}(a)}{d\ln a}\right|_{\text{inertial range}} =H^{(\phi)}(q)\left.\frac{dn^{(\phi)}(a)}{d\ln a}\right|_{\text{inertial range}}, \tag{35}$$

the ζ_q are mixing the scale a and order q dependences:

When measuring the ζ_q, a q difference between phases is observed that actually traces back to a difference in scale a. Therefore, the ζ_q's are confusing quantities to look at. They point to a difference in intermittency between phases but relate it to a q dependence while it is due to a a dependence. This is because the behavior $n(a)=\ln a$ is a priori assumed to strictly hold, though it is only approximately observed. Finally, since there is no sensitivity of the phases to q, one cannot conclude that a phase is closer to K41 than another, a question which would only make sense if strict scale invariance was observed.

A last remark is that although scale invariance is not observed over the entire range of scales, we observe that, within the inertial range, it is better verified for the filament phase than for the background one. Indeed we observe that the speed of deformation along the scales $dn(a)/d\ln(a)$, that is the rate at which the elementary block of the cascade is applied, is kept constant through the inertial range for the filaments, while it varies in the background unstructured phase. This raises the question of possible relationships between the geometrical properties of flow structures and scaling.

V. CONCLUSION

In this work, we have analyzed some scaling properties of turbulence and their relations to the existence of filamentary vortices in the flow thanks to the log-infinitely divisible cascade model. This model does not a priori assume exact scale invariance or pure power laws but naturally allows the observed departure from pure power laws to take place within the model. In the cascade framework, K41 assumptions imply both that scale invariance is valid and that the ζ_q are a linear function of q. Despite the fact that it is commonly accepted that the structure functions may significantly differ from pure power laws, most of the models proposed after K41 (log-normal, multifractal, . . .) question the linearity of the ζ_q but still maintain the scale invariance assumption. When it comes to experimental validation, they have to cope with the fact that scale invariance is not strictly observed. In the log-infinitely divisible cascade model, the functional forms of the functions ζ_q and $n(a)$ do not need to be a priori assumed. Therefore, this model is versatile and constitutes a relevant alternative to the usual scaling analysis.

Using this framework, we have shown that the existence of a cascade process in itself is not due to the presence of filaments. Filaments, yet, do influence statistical intermittency but not through the dependence of structure function exponents with the order of the structure function, as commonly proposed. The filaments do not act on the elementary step of the cascade that has universal characteristics, but rather on the speed rate at which the steps are made to develop the cascade. Moreover, we have shown how and why exponents of structure functions may be misleading quantities to look at when studying intermittency.

Finally, we emphasize the fact that the use of wavelet coefficients rather than increments played a key role in this analysis. Wavelets efficiently generalize increments in the analysis of the properties of the data at a given time scale as well as in the study of their scaling properties: They have better signal processing, statistical, and computational abilities.

ACKNOWLEDGMENTS

We are pleased to acknowledge fruitful discussions with S. Fauve, Y. Couder, B. Castaing, C. Baudet, and E. Levêque.

[1] M.-E. Brachet, ''Géométrie des structures à petite échelle dans le vortex de Taylor-Green,'' C. R. (Dokl.) Acad. Sci. URSS **311**, 775 (1990).
[2] W. T. Ashurst, A. R. Kerstein, R. M. Kerr, and G. H. Gibson, ''Alignment of vorticity and scalar gradient with strain rate in simulated Navier–Stokes turbulence,'' Phys. Fluids **30**, 2343 (1987).
[3] A. Tsinober, E. Kit, and T. Dracos, ''Experimental investigation of the field of velocity gradients in turbulent flows,'' J. Fluid Mech. **242**, 169 (1992).
[4] L. Shtilman, M. Spector, and A. Tsinober, ''On some kinematic versus dynamic properties of homogeneous turbulence,'' J. Fluid Mech. **247**, 65 (1993).
[5] B. Andreotti, ''Studying Burgers' models to investigate the physical meaning of the alignments statistically observed in turbulence,'' Phys. Fluids **9**, 735 (1997).
[6] F. Belin, J. Maurer, P. Tabeling, and H. Willaime, ''Observation of intense filaments in fully developed turbulence,'' J. Phys. II **6**, 573 (1996).
[7] P. Abry, S. Fauve, P. Flandrin, and C. Laroche, ''Analysis of pressure fluctuations in swirling turbulent flows,'' J. Phys. II **4**, 725 (1994).
[8] G. Stolovitzky, J.-L. Aider, and J. E. Wesfreid, ''Coherent structures and conditional statistics in inhomogeneous turbulent mixing,'' Phys. Rev. Lett. **78**, 4398 (1997).
[9] R. Camussi and G. Guj, ''Orthonormal wavelet decomposition of turbulent flows: Intermittency and coherent structures,'' J. Fluid Mech. **348**, 177 (1997).
[10] S. Fauve, C. Laroche, and B. Castaing, ''Pressure fluctuations in swirling turbulent flows,'' J. Phys. II **3**, 271 (1993).
[11] O. Cadot, S. Douady, and Y. Couder, ''Characterization of the low-pressure filaments in a three dimensional turbulent shear flow,'' Phys. Fluids **7**(3), 630 (1995).
[12] E. D. Siggia, ''Numerical study of small scale intermittency in three dimensional turbulence,'' J. Fluid Mech. **107**, 375 (1981).
[13] S. Douady, Y. Couder, and M.-E. Brachet, ''Direct observation of intense vorticity filaments in turbulence,'' Phys. Rev. Lett. **67**, 983 (1991).
[14] A. Pumir, ''A numerical study of pressure fluctuations in three-dimensional, incompressible, homogeneous, isotropic turbulence,'' Phys. Fluids **6**, 2071 (1994).
[15] S. Kida and K. Okhitani, ''Spatiotemporal intermittency and instability of a forced turbulence,'' Phys. Fluids A **4**, 1018 (1992).
[16] A. Vincent and M. Meneguzzi, ''The spatial structure and statistical properties of homogeneous turbulence,'' J. Fluid Mech. **225**, 1 (1991).
[17] B. Dernoncourt, J.-F. Pinton, and S. Fauve, ''Experimental study of vorticity filaments in a turbulent swirling flow,'' Physica D **117**, 181 (1998).
[18] E. Villermaux, B. Sixou, and Y. Gagne, ''Intense vortical structures ingrid-generated turbulence,'' Phys. Fluids **7**, 2008 (1995).
[19] R. Verzicco and J. Jimenez,''On the survival of nonuniform vortex filaments in turbulence'' (preprint).
[20] J.-F. Pinton, F. Chillà, and N. Mordant, ''Intermittency in the closed flow between coaxial corotating disks,'' Eur. J. Mech. B/Fluids **17**, 535 (1998).
[21] J. Jimenez, A. A. Wray, P. G. Saffman, and R. S. Rogallo, ''The structure of intense vorticity in isotropic turbulence,'' J. Fluid Mech. **255**, 65 (1993).
[22] A. Arnéodo, F. Argoul, E. Bacry, and J.-F. Elezgaray, J. Muzy, *Ondelettes, multifractales et turbulences* (Diderot, Editeur des Sciences et des Arts, Paris, 1995).
[23] P. Abry, *Ondelettes et Turbulence - Multirésolutions, Algorithmes de Décomposition, Invariance d'Echelle et Signaux de Pression* (Diderot, Editeur des Sciences et des Arts, Paris, 1997).
[24] M. Farge, N. Kevlahan, V. Perrier, and E. Goirand, ''Wavelets and turbulence,'' in *Proceedings of the IEEE,* Vol. 84, pp. 639–669 (1996).
[25] P. Abry, P. Flandrin, M. Taqqu, and D. Veitch, in *Wavelets for the analysis, estimation and synthesis of scaling data* (Wiley Interscience, New

York, 1999). To appear in Self Similar Network Traffic and Performance Evaluation.
[26]P. Abry, P. Gonçalvès, and P. Flandrin, in ''Wavelets, spectrum estimation and 1/*f* processes,'' in *Wavelets and Statistics, Lecture Notes in Statistics* (Springer-Verlag, New York, 1995), Chap. 103.
[27]P. J. Zandbergen and D. Dijkstra, ''von Kármán swirling flows,'' Annu. Rev. Fluid Mech. **19**, 465 (1987).
[28]J. Maurer, P. Tabeling, and G. Zocchi, ''Statistics of turbulence between two counter rotating discs in low temperature helium gas,'' Europhys. Lett. **26**, 31 (1994).
[29]J.-F. Pinton and R. Labbé, ''Correction to taylor hypothesis in swirling flows,'' J. Phys. II **4**, 1461 (1994).
[30]G. Comte-Bellot, ''Hot-wire anemometry,'' Annu. Rev. Fluid Mech. **8**, 209 (1976).
[31]R. Labbé, J.-F. Pinton, and S. Fauve, ''Power fluctuations in turbulent swirling flows,'' J. Phys. II **6**, 1099 (1996).
[32]Y. Gagne, ''Etude expérimentale de l'intermittence et des singularités dans le plan complexe en turbulence développée,'' Thèse de doctorat d'etat, Université Scientifique et Médicale et Inst. Nat. Poly. de Grenoble (1987).
[33]A. Arnéodo, E. Bacry, and J. F. Muzy, ''Singularity spectrum of fractal signals from wavelet analysis: Exact results,'' J. Stat. Phys. **70**, 635 (1994).
[34]Olivier Cadot, ''Etude des structures de basse pression dans la turbulence développée,'' Thèse de doctorat, Université Denis Diderot Paris 7, 1995.
[35]S. Roux, J.-F. Muzy, and A. Arnéodo, ''Detecting vorticity filaments using wavelet analysis: About the statistical contribution of vorticity filaments to intermittency in swirling turbulent flows,'' Eur. Phys. J. A **8**, 301 (1998).
[36]P.-O. Amblard, J.-L. Lacoume, and J. Brossier, ''Transient detection, higher-order time-frequency distributions and the entropy,'' in *Proceedings IEEE SP Workshop on Higher-Order Stat., Lake Tahoe, USA,* pp. 265–269 (1993).
[37]P. O. Amblard and J. M. Brossier, ''Adaptive estimation of the fourth-order cumulant of a white stochastic process,'' Signal Process. **42**(1), 37 (1995).
[38]D. Snyder and M. I. Miller, *Random point processes in time and space* (Springer Verlag, Berlin, 1991).
[39]F. Moisy, Investigation of low-pressure filaments using cavitation, unpublished internal report at Cornell University, collaboration with A. La Porta, G. Voth and E. Bodenschatz (1998).
[40]S. Douady and Y. Couder, ''On the dynamical structures observed in 3D turbulence,'' in *Turbulence in extended systems,* edited by R. Benzi, C. Basdevant, and S. Ciliberto (Nova Science, Commack, NY, 1993), pp. 3–17.
[41]P. Chainais, ''Etude des Structures de Basse Pression dans un Ecoulement Turbulent,'' Dea report, Laboratoire de Physique, ENS Lyon, 1997, unpublished.
[42]A. N. Kolmogorov, (a) dissipation of energy in the locally isotropic turbulence, (b) the local structure of turbulence in incompressible viscous fluid for very large reynolds number, (c) on degeneration of isotropic turbulence in an incompressible viscous liquid, in *Turbulence, Classic papers on statistical theory*, edited by S. K. Friedlander and L. Topper (Interscience, 1941), pp. 151–161.
[43]A. S. Monin and A. M. Yaglom, *Statistical Fluid Mechanics* (M.I.T., Cambridge, MA, 1975).
[44]R. Benzi, S. Ciliberto, R. Tripicione, C. Baudet, and F. Massaioli, ''Extended self similarity in turbulent flows,'' Phys. Rev. E **48**, R29 (1993).
[45]T. von Kŕmán and L. Howarth, ''On the statistical theory of isotropic turbulence,'' Proc. R. Soc. London, Ser. A **164**, 192 (1938).
[46]I. Daubechies, *Ten lectures on wavelets* (SIAM, Philadelphia, PA, 1992).
[47]S. Mallat, *A Wavelet Tour of Signal Processing* (Academic, New York, 1998).
[48]The theoretical and practical implications of this rewriting of the WSF in the DWT are under investigations and will be detailed elsewhere.
[49]B. Mandelbrot, ''Intermittent turbulence in self-similar cascades: divergence of high moments and dimension of the carrier,'' J. Fluid Mech. **62**, 331 (1974).
[50]U. Frisch and G. Parisi, in ''Fully developed turbulence and intermittency,'' in *Proceedings of Int. School on Turbulence and predictability in Geophysical Fluid Dynamics and Climate Dynamics*, edited by M. Ghil, R. Benzi, and G. Parisi (North-Holland, Amsterdam, 1985), p. 84.
[51]B. Castaing, Y. Gagne, and E. Hopfinger, ''Velocity probability density functions of high Reynolds number turbulence,'' Physica D **46**, 177 (1990).
[52]J. F. Arnéodo, A. Muzy, and S. Roux, ''Experimental analysis of self-similarity and random cascade processes: Application to fully developed turbulence data,'' J. Phys. II **7**, 363 (1997).
[53]P. Abry and D. Veitch, ''Wavelet analysis of long-range dependent traffic,'' IEEE Trans. Inf. Theory **44**(1), 2 (1998).
[54]G. Amati, F. Toschi, S. Succi, and R. Piva, ''Scaling exponents in turbulent channel flow,'' in *Advances in Turbulence VII* (Kluwer, Dordrecht, 1998), pp. 159–162.
[55]B. Andreotti, Y. Couder, and S. Douady, ''Experimental investigation of the turbulence near a large scale vortex,'' Eur. J. Mech. B/Fluids **17**(4), 451 (1998).
[56]H. Kahalerras, Y. Malécot, Y. Gagne, and B. Castaing, ''Intermittency and Reynolds Number,'' Phys. Fluids **10**(4), 910 (1998).
[57]R. Camussi and G. Guj, ''Statistical analysis of local turbulent energy fluctuations,'' J. Fluid Mech. **382**, 1 (1999).
[58]A. Arneodo, C. Baudet, R. Benzi, B. Castaing, R. Chavarria, S. Ciliberto, F. Chilla, B. Dubrulle, B. Hebral, J. Herweijer, J. Maurer, J.-F. Muzy, A. Noullez, J. Peinke, W. van de Water, and H. Willaime, ''Structure functions in turbulence, in various flow configurations, at Reynolds number between 30 and 5000, using extended self-similarity,'' Europhys. Lett. **34**(6), 411 (1996).
[59]E. Gaudin, B. Protas, S. Guyon-Durand, Wojciechowski, and J. E. Wesfreid, ''Spatial properties of velocity structure functions in turbulent wave flows,'' Phys. Rev. E **57**, R9 (1998).
[60]Y. Malécot, ''Intermittence en turbulence 3D: statistiques de la vitesse et de la vorticité,'' Thèse de doctorat, Université Joseph Fourier - Grenoble I, 1998.
[61]Y. Malécot, Cl. Auriault, H. Kahalerras, Y. Gagne, O. Chanal, B. Chabaud, and B. Castaing, ''A statistical estimator of turbulence intermittency in physical and numerical experiments'' (preprint).
[62]G. Ruiz-Chavarria, S. Ciliberto, C. Baudet, and E. Levêque, ''Scaling properties of velocity field in a turbulent boundary layer'' (preprint).